Event-Triggered Control for Servo Motor Systems Based on Fully Actuated System Approach and Dynamical Compensator

Ping Li, *Member, IEEE*, Guangren Duan, *Fellow, IEEE*, Bi Zhang, and Yuzhong Wang, *Member, IEEE*

***Abstract*—This article studies the event-triggered control (ETC) of servo motor systems based on fully actuated system (FAS) approach. The dynamics of servo systems is first simplified as a second-order FAS model, with which the control law can be synthesized for a desired tracking error dynamics in a very simple and straightforward way. To save the communication resource in networked control system (NCS), an ETC scheme is applied with a fixed threshold strategy, and a hyperbolic tangent function is employed to guarantee the exponential stability of the control system. Unfortunately, various uncertainties and disturbances in actual systems may severely degrade the tracking accuracy. To overcome this issue, a general dynamical compensator is utilized to better suppress the unknown disturbances. Furthermore, the stability of the control system is analyzed in the presence of parameter uncertainties. Simulation experiments are implemented on a practical servo motor with NCS to verify the effectiveness and superiority of the proposed control scheme.**

***Index Terms*—Dynamical compensator, event-triggered control (ETC), fully actuated system (FAS) approach, servo motor systems.**

Received 26 June 2024; revised 13 October 2024; accepted 24 November 2024. This work was supported in part by the National Natural Science Foundation of China under Grant 62203206 and Grant 62403234; in part by the Basic Science Center Program of the National Natural Science Foundation of China under Grant 62188101; in part by Guangdong Provincial Natural Science Foundation under Grant 2024A1515011648; in part by Shenzhen Key Laboratory of Control Theory and Intelligent Systems under Grant ZDSYS20220330161800001; in part by Shenzhen Science and Technology Innovation Commission under Grant JSGG20220831110605009 and Grant JCYJ20210324115413036; and in part by the Shenzhen Science and Technology Program under Grant KQTD20221101093557010. *(Corresponding authors: Guangren Duan; Yuzhong Wang.)*

Ping Li is with the Shenzhen Key Laboratory of Control Theory and Intelligent Systems, School of System Design and Intelligent Manufacturing, Southern University of Science and Technology, Shenzhen, Guangdong 518000, China (e-mail: lip3@sustech.edu.cn).

Guangren Duan is with the Center for Control Science and Technology, Southern University of Science and Technology, Shenzhen 518055, China, and also with the Center for Control Theory and Guidance Technology, Harbin Institute of Technology, Harbin 150001, China (e-mail: duangr@sustech.edu.cn).

Bi Zhang is with the Department of Mechanical and Energy Engineering, Southern University of Science and Technology, Shenzhen 518055, China (e-mail: zhangb@sustech.edu.cn).

Yuzhong Wang is with the Department of Electronic and Electrical Engineering, University of Hong Kong, Hong Kong 999077, China (e-mail: wyzmath@hku.hk).

Digital Object Identifier 10.1109/TIE.2024.3515273

I. Introduction

SERVO motors play a pivotal role in automation applications due to their outstanding performance in precise control and efficient energy use [1], [2], [3]. With the rapid development of economy and society, the demand for the high-performance automation equipment with complex functions is urgently increasing. For example, humanoid robots need a large number of servo motors to achieve the compliant operation. On the one hand, various of embedded systems have been widely applied to facilitate the controller design of robotics. On the other hand, the implementation of complex functions involves a lot of data communication. Traditionally, the time-scheduled sampling control architecture periodically updates and transmits signals, which is practically prohibitive due to the limitation of communication resources [4]. Event-triggered control (ETC) has been proven to be an efficient scheme to relieve the network communication burden, but it may degrade the quality of the control system. In addition, actual systems inevitably suffer from modeling errors due to uncertainties and disturbances [5], which may seriously deteriorate the control accuracy. It is still a challenge task to obtain the high performance of ETC for servo motor systems in a simple practical way.

There is no doubt that PID control technique has remained absolutely dominant for servo motor systems in the field of industrial applications by virtue of its many benefits such as simple principle and structure, easy operation, straightforward parameter tuning, reliable and robust performance [6]. Many design methods have been applied to explore the optimization of PID controllers, liking Ziegler-Nichols step response method [7], internal model principle [8], pole placement technique [9], linear quadratic regulation approach [10], to name but a few. To tackle the control issues of uncertainties, sliding mode control (SMC) has gained a lot of attention in the past decades [11], [12]. It has a strong control ability to eradicate the effect of uncertain dynamics via the sign control law, as well inherits almost all the advantages of PID control. In addition, advanced and intelligent control schemes, such as robust adaptive control [13], active disturbance rejection control (ADRC) [3], fuzzy-logic control [14], neural network learning control [15], have been widely applied to servo motor systems. It should be noted that most of the existing methods are based on the fixed-time sampling control strategy.

In recent years, networked control system (NCS) has become popular in the field of industrial control [16]. However, the

transmission load limitation for network communication must be considered. Compared with the traditional control scheme with periodic sampling, ETC can greatly save communication resources for that the process data are sent or received only when the predesigned triggering conditions are satisfied [17]. Since it helps avoid unnecessary consumption of the communication resource and can ensure an acceptable control performance simultaneously, ETC scheme has been broadly utilized in servo motion systems. For instance, the work in [18] proposes an ADRC approach for the servo control of DC torque motors based on ETC scheme. In [19], extended state observer (ESO) is designed to dispose of the control issues of uncertainties and disturbances in the motor systems with ETC mechanism via a high-gain approach. In [20], a proportional–integral ETC strategy is constructed for DC torque motors with NCS under unmatched uncertainties. In [21], an adaptive output feedback controller is proposed based on fuzzy observer and ETC scheme to tackle the issues of state constraints/time-delay and nonlinear hysteresis of servo motion systems.

To handle uncertainties and disturbances in servo systems with ETC scheme, two main approaches are adopted in existing methods: one is the adaptive control and the other is the observer-based control. Adaptive fuzzy control or neural network control methods own more potential capability to improve the control quality through approximation technique, but they are not favored by practical users due to the design complexity with more tuning parameters and more strict stability conditions. Observer-based approach (e.g. ESO) treats all the uncertain dynamics as a lumped disturbance for estimation and compensation, which can attenuate the harmful effect of unknown disturbances but may suffer from the problem of robustness stability. In addition, almost all the existing methods are based on first-order state-space approach, which is convenient for the analysis and estimation of states, but probably not the best solution for the control laws [22].

To overcome the drawback of state-space approach, a novel fully actuated system (FAS) approach is originally proposed by Duan on account of the second-order or high-order dynamics of actual systems [22], [23], [24]. Its core idea is to derive a mathematical FAS model for the considered system based on differential homeomorphism transformation, which can establish a balanced ratio of control inputs to system outputs. The full-actuation property ensures a more effective and convenient control strategy to obtain precise and desired system responses. Due to the significance in theory and practice, FAS approach has been widely applied in many applications like aerospace [25], [26] and robotics [27]. More application research results can be found in [28]. Particularly, a high-order FAS approach is applied in [29] for position control of servo motors, and in [30] for flexible servo systems. However, it is rare to investigate the FAS approach of servo motor systems with ETC scheme.

Inspired by the above observations, this article presents an ETC scheme for position control of servo motor systems by using FAS approach. In the proposed control strategy, a second-order FAS model is first formulated for servo motor systems by ignoring the electrical subsystem. Then, a simple ETC scheme with a fixed triggering threshold is applied to save the communication resource of NCS. Based on the FAS approach and the ETC scheme, a composite controller is designed for trajectory tracking. Furthermore, a dynamical compensator (DCr) is utilized to improve the control accuracy under uncertainties and disturbances. To the authors' best knowledge, it is the first time to apply FAS and DCr approaches for the ETC scheme of servo motor systems. The results are concise and elegant. The potential outcome is that the proposed approach can be applied to achieve a high control performance for the embedded system with limited resources, which can significantly reduce the cost while maintaining a well performance requirement. The main contributions of this article can be listed as follows:

1) A new control framework is proposed for the position tracking of servo motor systems based on FAS approach and ETC scheme, in which the control law can be synthesized in a simple and intuitive way to achieve a desired exponential convergence property.
2) A general p-order DCr is designed to introduce additional design degrees of freedom (DOFs) for the high-accuracy tracking control of servo systems under disturbances, which can avoid the practical problems associated with the high control gains.
3) Last but not least, the stability of the proposed approach is analyzed in the presence of parameter uncertainties, which provides the sufficient conditions for the robust stability of the control system. The effectiveness of the proposed control scheme has been verified by simulation experiments on a practical servo motor with NCS.

The rest of this article is organized as follows. In Section II, the system model of servo motors is established and the control goal is put forward. Section III presents the main results including the controller design and the stability analysis. The results of simulation experiments are shown in Section IV, followed by the concluding remark in Section V.

II. System Model and Problem Formulation

The control plant in this article is a servo motor system, which is made up of the mechanical subsystem

$$\begin{cases} \dfrac{d\theta}{dt} = \omega \\ J_m \dfrac{d\omega}{dt} = T_m - B_m\omega - T_L \end{cases} \tag{1}$$

and the electrical subsystem

$$\begin{cases} L_d \dfrac{di_d}{dt} = -R_a i_d + L_q i_q \omega + u_d \\ L_q \dfrac{di_q}{dt} = -R_a i_q - L_d i_d \omega - \psi_f \omega + u_q \\ T_m = 1.5 n_p \left(\psi_f + (L_d - L_q) i_d\right) i_q \end{cases} \tag{2}$$

where θ and ω denote the angular position and angular velocity, respectively; J_m is the motor inertia and B_m is the coefficient of viscous friction; T_m and T_L are respectively the motor driving torque and the load disturbance; L_d, i_d and u_d are respectively the stator inductance, stator current and stator voltage of d-axis; L_q, i_q and u_q are respectively the counterparts of q-axis; R_a is

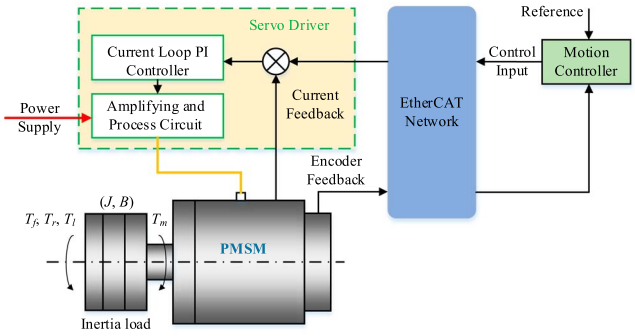

Fig. 1. Diagram of the servo motor with NCS.

the stator resistance; n_p is the number of pole pairs; ψ_f is the flux linkage.

Fig. 1 displays the diagram of the servo motor with NCS. Since the electrical time constant is much smaller than the mechanical time constant, the dynamics of the internal current control loop can be ignored to simplify the controller design of outer position loop [29]. Therefore, the control input u can be nearly equal to the motor driving torque T_m, i.e.

$$u \approx T_m. \tag{3}$$

Then, the model of servo motor system presented in (1) and (2) can be simplified into

$$\dot{\boldsymbol{x}} = \boldsymbol{A}\boldsymbol{x} + \boldsymbol{B}(u - T_L) \tag{4}$$

with

$$\boldsymbol{A} = \begin{bmatrix} 0 & 1 \\ 0 & -a_1 \end{bmatrix}; \boldsymbol{B} = \begin{bmatrix} 0 \\ b_0 \end{bmatrix}$$

where $\boldsymbol{x} \triangleq [x_1\ x_2]^T = [\theta\ \omega]^T$ denotes the vector of system states, $a_1 = B_m/J_m$ and $b_0 = 1/J_m$ are the system parameters.

By using the variable elimination method, a second-order FAS model of the system (4) can be obtained as

$$\ddot{x}_1(t) + a_1\dot{x}_1(t) = b_0 u(t) + d_1 \tag{5}$$

where $d_1 = -T_L/J_m$.

The control objective is to design an ETC scheme for the servo motor system presented in (1) and (2) such that the actual position θ can precisely track a desired trajectory θ_d under various uncertainties and disturbances.

Lemma 1 [31]: For a given continuous function $\epsilon(t)$ meeting $\epsilon(t) > 0$ and $\int_0^\infty \epsilon(\tau)d\tau \le \zeta < \infty$, ζ is a constant, the hyperbolic tangent function $\tanh(\cdot)$ satisfies

$$|\rho| - \rho\tanh\left(\frac{\rho}{\epsilon(t)}\right) \le \kappa\epsilon(t) \tag{6}$$

where $\rho \in \mathbb{R}$, $|\rho|$ denotes the absolute value of ρ, $\kappa = 0.2875$.

III. Controller Design

A. FAS Approach Based on ETC Scheme

In this article, a fixed threshold scheme is employed for ETC, in which the triggering condition for the update of control input is designed as

$$t_{k+1} = \inf\left\{t > t_k : \ |e_u(t)| \ge \sigma\right\} \tag{7}$$

where t_k is the kth triggering instant with $t_0 = 0$, σ is the designed trigger threshold, $e_u(t) \triangleq u(t) - u(t_k)$ denotes the control deviation between the current instant and the last triggering instant.

Based on FAS approach and ETC scheme, the control law for trajectory tracking can be synthesized as

$$u = u_{fb} + u_{ff} + u_e \tag{8}$$

where u_{fb} denotes the closed-loop controller, u_{ff} denotes the feedforward compensation controller, u_e is the control effort to handle the effect of ETC.

Based on the FAS model (5), u_{fb} and u_{ff} can be explicitly solved as

$$u_{fb} = -k_1\dot{e}_1 - k_0 e_1 \tag{9}$$

and

$$u_{ff} = \frac{1}{b_0}(\ddot{x}_{1d} + a_1\dot{x}_{1d}) \tag{10}$$

where $e_1 \triangleq x_1 - x_{1d}$ represents the tracking error.

Assume that $d_1 = 0$. Substituting the control law (8) with (9) and (10) to the system (5) yields

$$\dot{\boldsymbol{e}} = (\boldsymbol{A} - \boldsymbol{B}\boldsymbol{K_1})\boldsymbol{e} + \boldsymbol{B}u_e \tag{11}$$

where $\boldsymbol{e} \triangleq [e_1\ \dot{e}_1]^T$ is the vector of the tracking errors, $\boldsymbol{K_1} \triangleq [k_0\ k_1]$ is the gain vector.

Remark 1: The full-actuation property of FAS model allows to remove all the original dynamics and yield a desired linear closed-loop system with arbitrarily assignable eigenvalues. That possesses many merits such as simplicity, intuition and effectiveness on the controller design and analysis of servo motor systems, which is crucial for practical applications.

By properly choosing k_0 and k_1, we can arbitrarily assign the eigenvalues of the matrix $\boldsymbol{A} - \boldsymbol{B}\boldsymbol{K_1}$. Particularly, design the characteristics polynomial of (11) as

$$\lambda_c(s) = (s + \lambda_1)(s + \lambda_2) \tag{12}$$

where s denotes the Laplace operator, λ_1 and λ_2 are different positive constants. Then the control gains k_0 and k_1 can be explicitly solved as

$$k_0 = \frac{1}{b_0}\lambda_1\lambda_2; k_1 = \frac{1}{b_0}(\lambda_1 + \lambda_2 - a_1). \tag{13}$$

Let $\boldsymbol{A}_{c1} \triangleq \boldsymbol{A} - \boldsymbol{B}\boldsymbol{K_1}$, there exists a nonsingular matrix $\boldsymbol{T}_1 \in \boldsymbol{R}^{2\times 2}$ such that

$$\boldsymbol{T}_1^{-1}\boldsymbol{A}_{c1}\boldsymbol{T}_1 = \boldsymbol{\Lambda}_1; \boldsymbol{\Lambda}_1 \triangleq \begin{bmatrix} -\lambda_1 & 0 \\ 0 & -\lambda_2 \end{bmatrix}. \tag{14}$$

Let $\boldsymbol{\eta}_1 \triangleq \boldsymbol{T}_1^{-1}\boldsymbol{e}$. Based on the event-triggered condition (7), a hyperbolic tangent function is applied to design u_e as

$$u_e = -\sigma\tanh\left(\frac{\boldsymbol{\eta}_1^T\boldsymbol{T}_1^{-1}\boldsymbol{B}\sigma}{e^{-\mu t}}\right) \tag{15}$$

where $\mu > 0$ is a designed parameter.

Let $\xi(t)=e_u(t)/\sigma$ for $t\in[t_k\ t_{k+1})$. It is clear that $\xi(t_k)=0$, and $\xi(t_{k+1})=\pm1$. The ETC law $u(t_k)$ can be formulated as

$$u(t_k)=u(t)-\sigma\xi(t). \tag{16}$$

Applying $u(t_k)$ instead of $u(t)$ into the system (5), and noting (15), yields

$$\dot{\boldsymbol{e}}=\boldsymbol{A}_{c1}\boldsymbol{e}-\boldsymbol{B}\left[\sigma\xi(t)+\sigma\tanh\left(\frac{\boldsymbol{\eta}_1^T\boldsymbol{T}_1^{-1}\boldsymbol{B}\sigma}{e^{-\mu t}}\right)\right]. \tag{17}$$

Theorem 1: For the system (5) under $d_1=0$, the ETC law (16), with u composed of u_{fb} (9), u_{ff} (10) and u_e (15), and the control gains in (13), guarantees the exponential stability.

Proof: Taking the derivative of $\boldsymbol{\eta}_1$, and noting the dynamics in (17), yields

$$\dot{\boldsymbol{\eta}}_1=\boldsymbol{\Lambda}_1\boldsymbol{\eta}_1-\boldsymbol{T}_1^{-1}B\left[\sigma\xi(t)+\sigma\tanh\left(\frac{\boldsymbol{\eta}_1^T\boldsymbol{T}_1^{-1}\boldsymbol{B}\sigma}{e^{-\mu t}}\right)\right]. \tag{18}$$

Let $V_1\triangleq(1/2)\boldsymbol{\eta}_1^T\boldsymbol{\eta}_1$ be the Lyapunov function. Its derivative can be given by

$$\dot{V}_1=\boldsymbol{\eta}_1^T\boldsymbol{\Lambda}_1\boldsymbol{\eta}_1-\boldsymbol{\eta}_1^T\boldsymbol{T}_1^{-1}\boldsymbol{B}\left[\sigma\xi(t)+\sigma\tanh\left(\frac{\boldsymbol{\eta}_1^T\boldsymbol{T}_1^{-1}\boldsymbol{B}\sigma}{e^{-\mu t}}\right)\right]. \tag{19}$$

It is clear from (14) that

$$\boldsymbol{\Lambda}_1\le-\lambda_{\min}\boldsymbol{I}_2, \tag{20}$$

where $\lambda_{\min}=\min(\lambda_1,\lambda_2)$, $\boldsymbol{I}_2$ is the identity matrix of order 2.

Applying the results in Lemma 1 and the inequality (20) to the expression (19) results in

$$\dot{V}_1\le-\lambda_{\min}\boldsymbol{\eta}_1^T\boldsymbol{\eta}_1+\kappa e^{-\mu t}. \tag{21}$$

For the given $\lambda_{\min}$ and μ, there exists a constant γ satisfying $0<\gamma\le2\lambda_{\min}$ and $\gamma\ne\mu$. Then, integrating (21) yields

$$V_1(t)\le e^{-\gamma t}V_1(0)+\frac{\kappa}{\gamma-\mu}(e^{-\mu t}-e^{-\gamma t}) \tag{22}$$

which suggests the result in Theorem 1.

Remark 2: It is impossible to completely compensate the original dynamics via FAS approach due to the parameter uncertainties and unknown disturbances in actual systems, which may generate a harmful effect on the tracking accuracy. To overcome this drawback, DCr is readily designed to suppress the effect of uncertain dynamics.

B. FAS Approach With DCr Based on ETC Scheme

According to [29], the feedback controller based on DCr is constructed for the FAS system (5) as follows:

$$\begin{cases}u_{fb}=-(\boldsymbol{K}_e\boldsymbol{e}+\boldsymbol{K}_z\boldsymbol{z})\\ \dot{\boldsymbol{z}}=-\boldsymbol{a}_z\boldsymbol{z}+\boldsymbol{b}_e\boldsymbol{e}\end{cases} \tag{23}$$

where $\boldsymbol{z}\in\boldsymbol{R}^p$ is the vector of control variables, $\boldsymbol{K}_e\in\boldsymbol{R}^2$ and $\boldsymbol{K}_z\in\boldsymbol{R}^p$ are the control gain vectors, $\boldsymbol{a}_z\in\boldsymbol{R}^{p\times p}$ and $\boldsymbol{b}_e\in\boldsymbol{R}^{p\times2}$ represent the matrices of parameters.

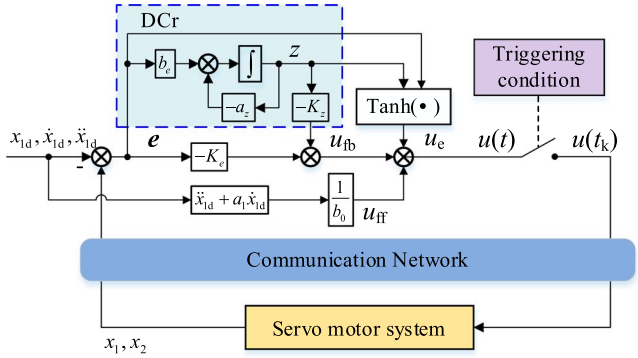

Fig. 2. Control block of the proposed approach.

Fig. 2 shows the control block of the proposed ETC scheme based on FAS and DCr approaches. Substituting the control law (8) with u_{fb} given by (23) and u_{ff} given by (10) into the system (5), yields

$$\begin{bmatrix}\dot{\boldsymbol{e}}\\ \dot{\boldsymbol{z}}\end{bmatrix}=\begin{bmatrix}\boldsymbol{A}-\boldsymbol{B}\boldsymbol{K}_e & -\boldsymbol{B}\boldsymbol{K}_z\\ \boldsymbol{b}_e & -\boldsymbol{a}_z\end{bmatrix}\begin{bmatrix}\boldsymbol{e}\\ \boldsymbol{z}\end{bmatrix}+\begin{bmatrix}\boldsymbol{B}\\ \boldsymbol{0}\end{bmatrix}(u_e-T_L). \tag{24}$$

Remark 3: Applying larger p can introduce more design DOFs to improve control performance, but makes the parameter tuning become more complex. As an illustrative example, only the DCr with $p=1$ is designed in this article. Let $\boldsymbol{z}=z_1$, $\boldsymbol{K}_e=[k_{e0}\ k_{e1}]$, $\boldsymbol{K}_z=k_{z0}$, $\boldsymbol{a}_z=a_{z0}$, $\boldsymbol{b}_e=[b_{e0}\ b_{e1}]$. Setting $u_e=0$, the FAS model of (24) can be given by

$$\dddot{e}_1+\beta_2\ddot{e}_1+\beta_1\dot{e}_1+\beta_0e_1=\dot{d}_1+a_{z0}d_1 \tag{25}$$

with

$$\begin{cases}\beta_0=(a_{z0}k_{e0}+b_{e0}k_{z0})b_0\\ \beta_1=a_{z0}a_1+(k_{e0}+a_{z0}k_{e1}+b_{e1}k_{z0})b_0\\ \beta_2=a_1+a_{z0}+k_{e1}b_0.\end{cases}$$

Design the desired characteristic polynomial of (25) as

$$\lambda_c(s)=(s+\lambda_1)(s+\lambda_2)(s+\lambda_3). \tag{26}$$

Let $\Upsilon\triangleq\ddot{e}_1+(\lambda_1+\lambda_2)\dot{e}_1+\lambda_1\lambda_2e_1$ be an output function. One has

$$G_\Upsilon(s)=\frac{e_1(s)}{\Upsilon(s)}=\frac{1}{(s+\lambda_1)(s+\lambda_2).} \tag{27}$$

Remark 4: It is clear from (27) that $G_\Upsilon(s)$ is a low-pass filter and e_1 is the filtered value of Υ, which satisfies $|e_1|\le(1/\lambda_1\lambda_2)|\Upsilon|$ via the Laplace transformation properties. The convergence of Υ to zero suggests the convergence of e_1 to zero.

Lemma 2: Given that $|d_1|\le d_{\max}$ and $|\dot{d}_1|\le D_{\max}$, the control law (8) with u_{fb} given by (23), u_{ff} given by (10), and $u_e=0$ ensures that the system (5) has a practical exponential stability. Furthermore, the error function Υ is bounded by

$$\Upsilon(t)\le e^{-\lambda_3 t}\Upsilon(0)+\frac{D_{\max}+a_{z0}d_{\max}}{\lambda_3}(1-e^{-\lambda_3 t}). \tag{28}$$

Proof: Taking the derivative of Υ, yields

$$\dot{\Upsilon}=\dddot{e}_1+(\lambda_1+\lambda_2)\ddot{e}_1+\lambda_1\lambda_2\dot{e}_1. \tag{29}$$

Substituting (25) into (29), one has

$$\begin{aligned}\dot{\Upsilon} &= -\lambda_3(\ddot{e}_1 + (\lambda_1+\lambda_2)\dot{e}_1 + \lambda_1\lambda_1 e_1) + \dot{d}_1 + a_{z0}d_1 \\ &= -\lambda_3\Upsilon + \dot{d}_1 + a_{z0}d_1. \end{aligned} \tag{30}$$

Integrating (30) over $[0\ t]$, yields

$$e^{\lambda_3 t}\Upsilon(t) - \Upsilon(0) = \int_0^t e^{\lambda_3\tau}(\dot{d}_1(\tau) + a_{z0}d_1(\tau))d\tau. \tag{31}$$

Applying $|d_1| \le d_{\max}$ and $|\dot{d}_1| \le D_{\max}$ to (31), it is easy to obtain the inequality (28). According to the definition in [3], the control system (5) possesses a practical exponential stability. The proof is completed.

Remark 5: It is clear from (28) that the upper bound of control error depends on the sum of $D_{\max}$ and $a_{z0}d_{\max}$ for the given $\lambda_i (i = 1,\ 2,\ 3)$. For that the variable d_1 and $\dot{d}_1$ are independent, setting $a_{z0} = 0$ can remove the contribution of $d_{\max}$ on the upper bound, and thus can improve the control accuracy.

By setting $a_{z0} = 0$, the feedback controller u_{fb} presented in (23) degrades into a PID controller, which can be expressed as

$$u_{fb} = -\frac{1}{b_0}\left(k_p e_1 + k_i\int e_1 dt + k_d\dot{e}_1\right) \tag{32}$$

where the control gains k_p, k_i, and k_d are given by

$$\begin{cases} k_p = \lambda_1(\lambda_2+\lambda_3) + \lambda_2\lambda_3 \\ k_i = \lambda_1\lambda_2\lambda_3, \\ k_d = \lambda_1 + \lambda_2 + \lambda_3 - a_1. \end{cases} \tag{33}$$

Substituting the control law (8) with u_{fb} in (32) and u_{ff} in (10) into the system (5) yields

$$\dot{\boldsymbol{E}} = \boldsymbol{A}_{c2}\boldsymbol{E} + \boldsymbol{B}_2 u_e. \tag{34}$$

where $\boldsymbol{E} \triangleq [z_1\ \boldsymbol{e}^T]^T$, $\boldsymbol{A}_{c2}$ and $\boldsymbol{B}_2$ are respectively given by

$$\boldsymbol{A}_{c2} = \begin{bmatrix} 0 & 1 & 0 \\ 0 & 0 & 1 \\ -k_i & -k_p & -(k_d + a_1) \end{bmatrix}; \boldsymbol{B}_2 = \begin{bmatrix} 0 \\ 0 \\ b_0 \end{bmatrix}.$$

Based on the assigned different eigen-values $-\lambda_1$, $-\lambda_2$ and $-\lambda_3$, there exists a nonsingular matrix $\boldsymbol{T}_2 \in \boldsymbol{R}^{3\times 3}$ such that

$$\boldsymbol{T}_2^{-1}\boldsymbol{A}_{c2}\boldsymbol{T}_2 = \boldsymbol{\Lambda}_2; \boldsymbol{\Lambda}_2 \triangleq \begin{bmatrix} -\lambda_1 & 0 & 0 \\ 0 & -\lambda_2 & 0 \\ 0 & 0 & -\lambda_3 \end{bmatrix}. \tag{35}$$

Let $\boldsymbol{\eta}_2 = \boldsymbol{T}_2^{-1}\boldsymbol{E}$. The ETC law u_e for the system (34) can be redesigned as

$$u_e = -\sigma\tanh\left(\frac{\boldsymbol{\eta}_2^T\boldsymbol{T}_2^{-1}\boldsymbol{B}_2\sigma}{e^{-\mu t}}\right). \tag{36}$$

Applying $u(t_k)$ in (16) instead of $u(t)$ to the FAS system (5), and noting (36), yields

$$\dot{\boldsymbol{E}} = \boldsymbol{A}_{c2}\boldsymbol{E} - \boldsymbol{B}_2\left[\sigma\xi(t) + \sigma\tanh\left(\frac{\boldsymbol{\eta}_2^T\boldsymbol{T}_2^{-1}\boldsymbol{B}_2\sigma}{e^{-\mu t}}\right)\right]. \tag{37}$$

Theorem 2: Given that $\dot{d}_1 = 0$, the ETC law (16), with u composed of u_{fb} (32), u_{ff} (10) and u_e (36), and the control gains in (33), guarantees that the system (5) has an exponential stability.

Proof: Taking the derivative of $\boldsymbol{\eta}_2$, and noting the dynamics in (37), yields

$$\dot{\boldsymbol{\eta}}_2 = \boldsymbol{\Lambda}_2\boldsymbol{\eta}_2 - \boldsymbol{T}_2^{-1}\boldsymbol{B}_2\left[\sigma\xi(t) + \sigma\tanh\left(\frac{\boldsymbol{\eta}_2^T\boldsymbol{T}_2^{-1}\boldsymbol{B}_2\sigma}{e^{-\mu t}}\right)\right]. \tag{38}$$

Define the Lyapunov function as $V_2 \triangleq (1/2)\boldsymbol{\eta}_2^T\boldsymbol{\eta}_2$. Its derivative can be given by

$$\begin{aligned}\dot{V}_2 = &\boldsymbol{\eta}_2^T\boldsymbol{\Lambda}_2\boldsymbol{\eta}_2 \\ &- \boldsymbol{\eta}_2^T\boldsymbol{T}_2^{-1}\boldsymbol{B}_2\left[\sigma\xi(t) + \sigma\tanh\left(\frac{\boldsymbol{\eta}_2^T\boldsymbol{T}_2^{-1}\boldsymbol{B}_2\sigma}{e^{-\mu t}}\right)\right]. \end{aligned} \tag{39}$$

It is clear from (35) that

$$\boldsymbol{\Lambda}_2 \le -\lambda'_{\min}\boldsymbol{I}_3, \tag{40}$$

where $\lambda'_{\min} = \min(\lambda_1, \lambda_2,\ \lambda_2)$, $\boldsymbol{I}_3$ is the identity matrix of order 3.

Applying the results in Lemma 1 and the inequality (40), the expression (39) satisfies

$$\dot{V}_2 \le -\lambda'_{\min}\boldsymbol{\eta}_2^T\boldsymbol{\eta}_2 + \kappa e^{-\mu t}. \tag{41}$$

For the given $\lambda'_{\min}$ and μ, there certainly exists a constant γ' satisfying $0 < \gamma' \le 2\lambda'_{\min}$ and $\gamma' \ne \mu$. Then, integrating (41) over $[0\ t]$ yields

$$V_2(t) \le e^{-\gamma' t}V_2(0) + \frac{\kappa}{\gamma' - \mu}\left(e^{-\mu t} - e^{-\gamma' t}\right) \tag{42}$$

which suggests the result in Theorem 2.

Remark 6: Under the time-varying disturbances satisfying $|d_1| \le d_{\max}$ and $|\dot{d}_1| \le D_{\max}$, the proposed control approach can only ensure the practical exponential stability instead of the exponential stability for the control system. It is easy to know from the result in Lemma 2 that the upper limit of the tracking error e_1 can be made small enough by properly choosing the parameters $\lambda_i,\ i = 1,\ 2,\ 3$.

Unfortunately, too large λ_i $(i = 1,\ 2,\ 3)$ may excite the high-frequency dynamics, such as discretization errors and current-loop dynamics, which has been ignored to simply the controller design and analysis. The parameter setting of λ_i $(i = 1,\ 2,\ 3)$ should make a trade-off between the control accuracy and the system sensitivity to the ignored high-frequency dynamics. Based on the step response or the bandwidth idea, the trial-and-error method is popular in practice to obtain the satisfactory control performance.

C. Stability Analysis Under Parameter Uncertainties

Let $d_1 = 0$. The state-space system (4) under parameter uncertainties can be rewritten as

$$\dot{\boldsymbol{x}} = (\boldsymbol{A} + \Delta\boldsymbol{A})\boldsymbol{x} + (\boldsymbol{B} + \Delta\boldsymbol{B})u \tag{43}$$

with

$$\Delta\boldsymbol{A} = \begin{bmatrix} 0 & 0 \\ 0 & -\tilde{a}_1 \end{bmatrix},\ \Delta\boldsymbol{B} = \begin{bmatrix} 0 \\ \tilde{b}_0 \end{bmatrix}$$

where $\tilde{a}_1$ and $\tilde{b}_0$ denote the parameter deviations of a_1 and b_0, respectively, satisfying

$$|\tilde{a}_1| \le \delta_a; |\tilde{b}_0| \le \delta_b. \tag{44}$$

Applying $u(t_k)$ in (16) instead of $u(t)$ with u_{fb} in (23) and u_e in (36) to (43) and noting that $\dot{\theta}_d = 0$ and $\ddot{\theta}_d = 0$, yields

$$\dot{\boldsymbol{E}} = (\boldsymbol{A}_{c2} + \Delta\boldsymbol{A}_{c2})E - (\boldsymbol{B}_2 + \Delta\boldsymbol{B}_2)\left[\sigma\xi(t) + \sigma\tanh\left(\frac{\boldsymbol{\eta}_2^T\boldsymbol{T}_2^{-1}\boldsymbol{B}_2\sigma}{e^{-\mu t}}\right)\right] \tag{45}$$

with $\Delta\boldsymbol{A}_{c2}$ and $\Delta\boldsymbol{B}_2$ given by

$$\Delta\boldsymbol{A}_{c2} = \begin{bmatrix} 0 & \boldsymbol{0} \\ 0 & \Delta\boldsymbol{A} \end{bmatrix} + \Delta\boldsymbol{B}_2\boldsymbol{K}_2, \Delta\boldsymbol{B}_2 = \begin{bmatrix} 0 \\ \Delta\boldsymbol{B} \end{bmatrix} \tag{46}$$

where $\boldsymbol{K_2} \triangleq (1/b_0)[k_p\ k_i\ k_d]$ denotes the vector of control gains.

Theorem 3: Given the boundary conditions in (44), the ETC law (16), with u composed of u_{fb} (32), u_{ff} (10) and u_e (36), and the control gains in (33), ensures the exponential stability of the uncertain system (43), if the following condition is satisfied:

$$\delta_2 + \delta_1\|\boldsymbol{K_2}\| < \frac{\lambda'_{\min}}{\|\boldsymbol{T}_2^{-1}\|\|\boldsymbol{T}_2\|}. \tag{47}$$

Proof: Under parameter uncertainties, the derivative of $\boldsymbol{\eta}_2$ can be rewritten as

$$\dot{\boldsymbol{\eta}}_2 = \boldsymbol{\Lambda}_2\boldsymbol{\eta}_2 + \Delta\boldsymbol{A}'_c\boldsymbol{\eta}_2 - \boldsymbol{T}_2^{-1}(\boldsymbol{B}_e + \Delta\boldsymbol{B}_e)\left[\sigma\xi(t) + \sigma\tanh\left(\frac{\boldsymbol{\eta}_2^T\boldsymbol{T}_2^{-1}\boldsymbol{B}_2\sigma}{e^{-\mu t}}\right)\right] \tag{48}$$

where $\Delta\boldsymbol{A}'_{c2} = \boldsymbol{T}_2^{-1}\Delta\boldsymbol{A}_{c2}\boldsymbol{T}_2$.

Then, the derivative of V_2 $\left(V_2 \triangleq (1/2)\boldsymbol{\eta}_2^T\boldsymbol{\eta}_2\right)$ can be obtained as

$$\dot{V}_2 = \boldsymbol{\eta}_2^T\boldsymbol{\Lambda}_2\boldsymbol{\eta}_2 + \frac{1}{2}\boldsymbol{\eta}_2^T(\Delta\boldsymbol{A}'_{c2}T + \Delta\boldsymbol{A}'_{c2})\boldsymbol{\eta}_2 - \frac{b_0 + \tilde{b}_0}{b_0}\boldsymbol{\eta}_2^T\boldsymbol{T}_2^{-1}\boldsymbol{B}_2\left[\sigma\xi(t) + \sigma\tanh\left(\frac{\boldsymbol{\eta}_2^T\boldsymbol{T}_2^{-1}\boldsymbol{B}_2\sigma}{e^{-\mu t}}\right)\right]. \tag{49}$$

Applying the conditions in (44) to the expression (46), one has

$$\|\Delta\boldsymbol{A}_{c2}\| \le \left\|\begin{bmatrix} 0 & \boldsymbol{0} \\ 0 & \Delta\boldsymbol{A} \end{bmatrix} + \begin{bmatrix} 0 \\ \Delta\boldsymbol{B} \end{bmatrix}\boldsymbol{K_2}\right\| \le \delta_a + \delta_b\|\boldsymbol{K_2}\| \tag{50}$$

which yields

$$\|\Delta\boldsymbol{A}'_{c2}\boldsymbol{T} + \Delta\boldsymbol{A}'_{c2}\| \le 2\|\boldsymbol{T}_2^{-1}\Delta\boldsymbol{A}_{c2}\boldsymbol{T}_2\| \le 2\|\boldsymbol{T}_2^{-1}\|(\delta_a + \delta_b\|\boldsymbol{K_2}\|)\|\boldsymbol{T}_2\|. \tag{51}$$

Applying (6) (35), (44) and (51) to (49) yields

$$\dot{\boldsymbol{V}}_2 \le -\left\{\lambda'_{\min} - (\delta_a + \delta_b\|\boldsymbol{K_2}\|)\|\boldsymbol{T}_2^{-1}\|\|\boldsymbol{T}_2\|\right\}\boldsymbol{\eta}_2^T\boldsymbol{\eta}_2 + \kappa\left(1 + \frac{\delta_b}{b_0}\right)e^{-\mu t}. \tag{52}$$

Let $\delta_0 = \lambda'_{\min} - (\delta_a + \delta_b\|\boldsymbol{K_2}\|)\|\boldsymbol{T}_2^{-1}\|\|\boldsymbol{T}_2\|$ and define $\kappa' = \kappa(1 + (\delta_b/b_0))$. It follows from (47) that $\delta_0 > 0$ and $\kappa' > 0$. For the given $\lambda'_{\min}$ and μ, there exists a constant γ'' satisfying $0 < \gamma'' \le 2\delta_0$ and $\gamma'' \ne \mu$. Integrating (52) over the interval $[0\ t]$ yields

$$\boldsymbol{V}_2(t) \le \boldsymbol{e}^{-\gamma'' t}\boldsymbol{V}_2(0) + \frac{\kappa'}{\gamma'' - \mu}(e^{-\mu t} - e^{-\gamma'' t}) \tag{53}$$

which implies that the result in Theorem 3 is true.

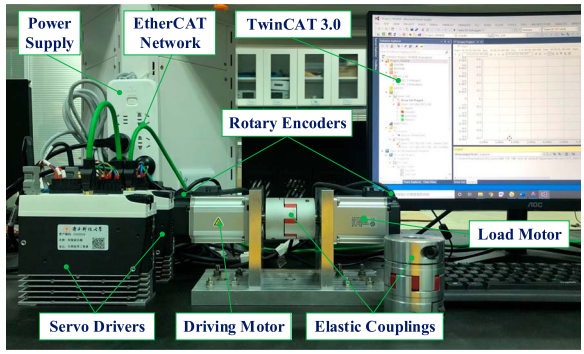

Fig. 3. Photograph of experiment platform.

Remark 7: Different from the common disturbance observer (DOB) or ESO, the proposed DCr is a model-free design method, in which only the system states are utilized for disturbance estimation and compensation. In addition, DCr is designed combining with the baseline controller to yield a desired closed-loop system via FAS approach, which can better deal with the control issues under uncertainties.

IV. Experiment Validation

A. Experiment Setup

Fig. 3 shows the experiment platform of servo motor system, in which two Panasonic ac servo motors with the product No. MSMF042L1U2M are applied. One is the driving motor for trajectory tracking control and the other is the load machine to generate various load disturbances. The matched servo drivers (product No. MBDLN25BE) are worked in torque control mode, which receive and send the digital data via the EtherCAT network communication protocol. The controller algorithm code is programmed in the industrial automation software TwinCAT 3, which is served as the master station in NCS and can offer the cycle update of 8 kHz. The parameters of system configuration can be found in [32].

In this experiment setup, the nominal values of the load inertia and the damping coefficient are given by $J = 9.6 \times 10^{-5}$ kg · m^2 and $B = 8.0 \times 10^{-4}$ Nm/(rad/s), respectively. It is clear that the mechanical time constant is $\tau_m = J/B = 0.12$. According to the result of identification experiment in [29], the identified model of the current-loop dynamics can be given by

$$G_c(s) = \frac{T_m(s)}{u(s)} = \frac{0.888}{0.000231s + 1}e^{-0.000812s}. \tag{54}$$

Applying the first-order Taylor ($e^{Ls} \approx 1 + Ls$) to approximate the time delay, it is easy to know that the time constant of the current-loop system is $\tau_e \approx 0.001$, which is much smaller than the mechanical time constant, i.e., $\tau_e \ll \tau_m$. Therefore, it is reasonable that the current-loop dynamics can be ignored for the position controller design and the property in (3) is satisfied.

B. Step Response Test

The step response performance is first tested, in which the step value of the position is set as 0.2 rad, and a step disturbance of 0.2 Nm is applied to the system by the load motor at 250 ms.

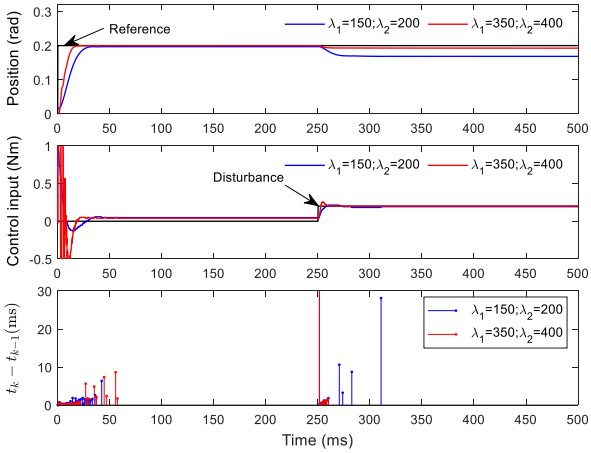

Fig. 4. Step response under ETC-FAS.

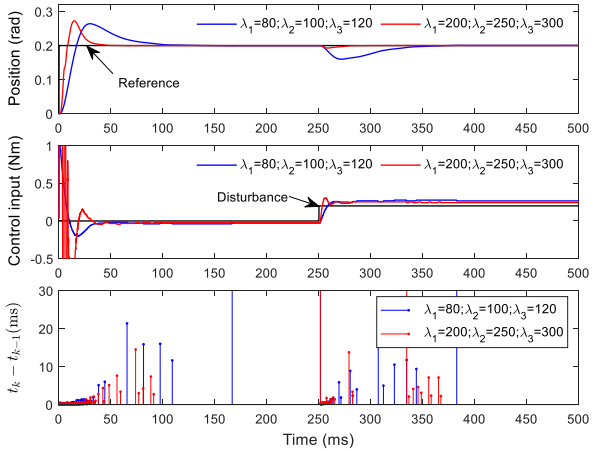

Fig. 5. Step response under ETC-FAS-DC.

The following two controllers with ETC scheme are designed for comparison.

1) *ETC-FAS*: This is the proposed ETC scheme based on FAS approach, in which the event-triggered condition in (7) and the synthesized control law u in (8) are applied, with u_{fb} given by (9), u_{ff} given by (10), u_e given by (15) and the control gains given by (13).
2) *ETC-FAS-DC*: This is the proposed ETC scheme based on FAS and DCr approaches, with the control framework presented in (7) and (8). The difference from ETC-FAS is that a first-order DCr ($p = 1$) is introduced in this control strategy, leading to that u_{fb} is given by (32), u_e is given by (36) and the control gains given by (33).

Based on the parametric design method, the control gains of each scheme can be explicitly solved by the desired eigenvalues of the closed-loop system. To better test the controller performance, two different sets of eigenvalues are applied to design the control gains of each control scheme: Set A1 ($\lambda_1 = 150$, $\lambda_2 = 200$) and Set A2 ($\lambda_1 = 350$, $\lambda_2 = 400$) in ETC-FAS, Set B1 ($\lambda_1 = 80$, $\lambda_2 = 100$, $\lambda_3 = 120$) and Set B2 ($\lambda_1 = 200$, $\lambda_2 = 250$, $\lambda_3 = 300$) in ETC-FAS-DC. The parameter tuning is based on trial-and-error method according to the transient performance of step response. For fair comparison, all the control schemes employ the same trigger threshold, which is set as $\sigma = 0.01$ Nm.

Fig. 4 shows the actual positions, control inputs and triggering intervals of the step response under ETC-FAS. Compared with Set A1, Set A2 achieves a faster rising time for the step reference and a smaller steady-state error under the constant disturbance, but more serious oscillations for control input. It suggests that applying larger control gains can improve the control accuracy in the presence of disturbances, but may excite the ignored high-frequency dynamics to cause the stability problem. In addition, the total number of triggers of Set A1 and Set A2 are respectively 88 and 159, occupying the percentage of 2.2% and 3.98% over the 4000 cycle sampling data at the experiment time of 500 ms. This can be attributed to that ETC selectively transmits system sampled data signals, which can significantly improve data transmission efficiency and reduce network bandwidth pressure.

Fig. 5 shows the results of step response under ETC-FAS-DCr. Similarly, applying larger eigenvalues can improve the control accuracy but impair the system stability. The total numbers of triggers of Set B1 and Set B2 are respectively 126 and 232, occupying the percentage of 3.15% and 5.8% over the total sampling data. It should be noted that ETC-FAS-DC can make the tracking error converge to zero under the constant disturbance, possessing an enormous superiority on disturbance rejection over ETC-FAS. This can be attributed to that the introduced DCr offers extra design DOF to better suppress the unknown disturbances, which can avoid the control problems associated with the high-gain scheme.

C. Robust Tracking Control

This subsection aims at testing the tracking accuracy of the proposed control approach under parameter uncertainties. The desired trajectory is designed as $\theta_d = 10(1 - e^{-t})(1 - \cos(2\pi t))$ rad, and the parameter uncertainty is implemented by replacing the inertia load with another one, in which the change of the moment of inertia is designed as $\Delta J \approx 1.6 \times 10^{-4}$ kg $\cdot$ m^2.

Based on the results of step response, the control gains of each scheme are designed by using the large eigenvalue sets, that is, $\lambda_1 = 350$, $\lambda_2 = 400$ in ETC-FAS and $\lambda_1 = 200$, $\lambda_2 = 250$, $\lambda_3 = 300$ in ETC-FAS-DC. Besides, a state-of-the-art ETC-based adaptive fault-tolerant control (ETC-AFTC) in [33] is added to enhance the persuasiveness of the proposed method, with the control parameters set as $k_1^0 = 1$, $k_1^\infty = 0.3$, $k_2^0 = k_2^\infty = 20$, $c_{11} = 0.003$, $c_{12} = 0.017$, $c_{21} = 0.005$, $c_{22} = 0.01$, $\gamma_1 = 10$, $\gamma_2 = 20$ and $\xi_1^0 = \xi_2^0 = 2.0$. Due to the lack of intuitive physical meaning, these parameters in ETC-AFTC are tuned by trial-and-error method. All the comparative controllers adopt the same fixed ETC scheme to part B of this section.

To evaluate the control accuracy and the communication efficiency, the maximum absolute error (MAE) of e_1, the integral absolute error (IAE) of e_1 and the percentage (PCT) of the

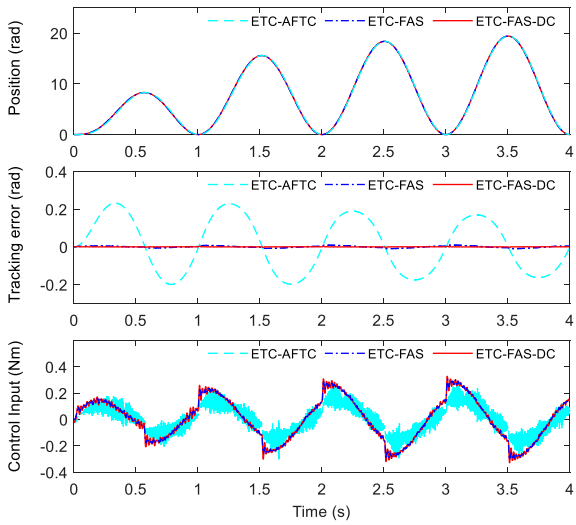

Fig. 6. Trajectory tracking test with uncertain J.

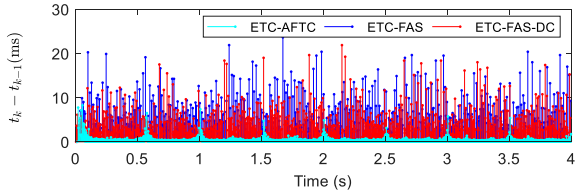

Fig. 7. Interval time of triggers under uncertain J.

triggering number n_{T} over the total sampling cycles n_{S} are applied as the performance indices, which are respectively formulated as

$$\mathrm{MAE} = \max\{e_1\} \tag{55}$$

$$\mathrm{IAE} = \int_0^t |e_1| dt \tag{56}$$

$$\mathrm{PCT} = \frac{n_{\mathrm{T}}}{n_{\mathrm{S}}} \times 100\%. \tag{57}$$

Compared with the performance metrics used in the benchmark methods, i.e., step response test, MAE can more directly measure the trajectory tracking accuracy under uncertainties and disturbances, which is the main goal of servo drive control system design. Since actual systems are very complex and subject to stochastic noises and perturbations, IAE and PCT can be used as the statistical performance indices to measure the control performance over a test period.

Figs. 6 and 7 show the experimental results under uncertain J, including actual positions, tracking errors, control inputs, and the interval time of triggers. The performance indices (MAE, IAE, and PCT) of the three controllers are presented in Table I. It is clear from these experimental results that compared with ETC-AFTC, both ETC-FAS and ETC-FAS-DC can greatly improve the tracking accuracy and reduce the number of triggering events. The reason is that ETC-AFTC is a model-free control strategy and the adaptive Nussbaum function can only ensure the bounded stability. In addition, the ignored high-frequency dynamics of servo system is more easily exited under ETC-AFTC, which results in serious system oscillations and more triggering events. Different from ETC-AFTC, FAS approach is a model-based control strategy, which can obviously improve the tracking accuracy by removing the original dynamics of servo system. Besides, the introduction of DCr offers additional control effort to improve the control performance of FAS, which can greatly attenuate the harmful effect of uncertainties such that a much better tracking accuracy can be obtained. It should be noted that the extra control effort via DCr may make the control law change more rapidly, resulting in that the triggering condition with a fixed threshold can be more easily met. Fortunately, both the two FAS approaches have reduced the control input updates by more than 96%, saving much more networked communication resources than ETC-AFTC. Therefore, the proposed approach possesses a huge advantage on the improvement of the tracking control performance over the state-of-the-art method.

TABLE I
PERFORMANCE INDICES UNDER UNCERTAINTY AND DISTURBANCE

Schemes	Uncertain J			Cosine Disturbance		
	MAE (rad)	IAE (rad)	PCT (%)	MAE (rad)	IAE (rad)	PCT (%)
ETC-AFTC	0.23	0.52	73.4	0.32	0.34	3.2
ETC-FAS	0.0098	0.016	2.2	0.045	0.049	2.4
ETC-FAS-DC	0.0039	0.0015	3.6	0.0028	0.0036	2.6

D. Disturbance Rejection Control

The experiment of disturbance rejection control is conducted in this subsection for further performance illustration. The cosine disturbance is produced by the load motor, which is designed as $T_L = 0.5(1 - \cos(\omega_d t))$ Nm. To better test the disturbance rejection performance, the desired trajectory is set as $\theta_d = 0$. The three control schemes (ETC-AFTC, ETC-FAS, and ETC-FAS-DC) are applied for test in this part, with the same control parameters to part C of this section.

Fig. 8 shows the output positions and control input torques under the cosine disturbance, in which the interval time of triggers $(t_k - t_{k-1})$ is presented in Fig. 9. Table I displays the corresponding MAE, IAE, and PCT. It can be seen that ETC-FAS and ETC-FAS-DC have respectively reduced the control input updates by 97.6% and 97.4%, which can better improve the utilization efficiency of communication resources than ETC-AFTC, which reduces the triggering events by 96.8%. In addition, under the time-varying disturbances, the MAEs of ETC-AFTC, ETC-FAS and ETC-FAS-DC are 0.34 rad, 0.045 rad, and 0.0028 rad, respectively. Obviously, ETC-FAS obtains a much better control accuracy than ETC-AFTC, while ETC-FAS-DC obtains a much better control accuracy than ETC-FAS. This demonstrates that the FAS approach adopted in ETC-FAS and ETC-FAS-DC can better suppress the unknown external disturbances than the adaptive fault tolerant control in ETC-AFTC. Besides, the introduction of DCr can significantly improve the disturbance rejection performance of the FAS

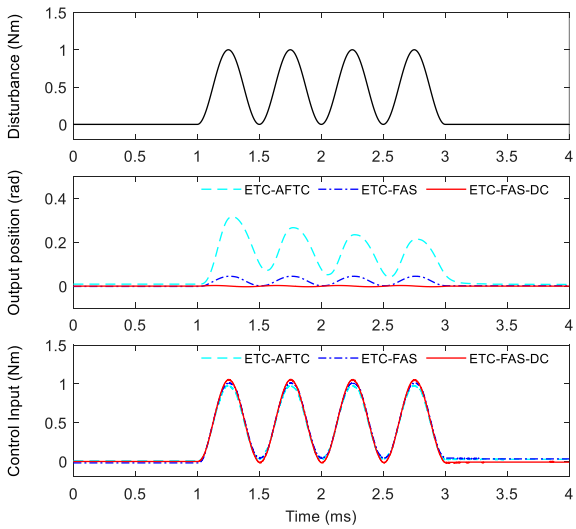

Fig. 8. Output regulation under cosine disturbance.

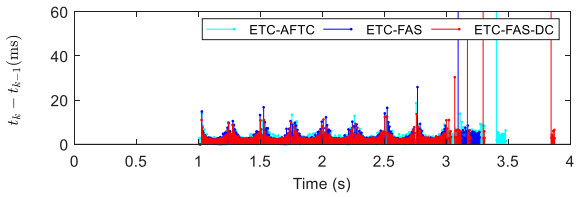

Fig. 9. Interval time of triggers under cosine disturbance.

approach. Also note that the update of control input may be triggered even if the load disturbance is removed. This can be attributed to the discontinuous friction force of servo systems, as well as the ignored high-frequency dynamics in practical applications.

V. Conclusion

In this article, a new ETC scheme is proposed for the high precision control of servo motor systems based on FAS and DCr approaches, which possess many merits such as simplicity, intuition, and effectiveness on controller design and analysis. Theoretical analysis guarantees the exponential convergence of the control system under parameter uncertainties. Simulation experiments have been conducted on a practical servo motor with NCS. The results show that the proposed ETC scheme can reduce the input communication data by more than 94%, saving the communication resource significantly. Besides, applying DCr to FAS approach can greatly improve the control accuracy of servo motor systems, especially under large uncertainties and disturbances. That provides a well verification for the practicability and superiority of the proposed approach.

In this article, the control input should be generated and monitored in real time in ETC scheme, which causes extra expenditure for practical applications. Future work will devote to exploring more efficient ETC schemes and applying the proposed approach for larger systems or different types of servo motors not discussed in this article.

References

[1] V. N. Hung, K. Suleimenov, N. Bao-Huy, V.-D. T. C. T. Minh, and D. T. Duc, "Dynamical delay unification of disturbance observation techniques for PMSM drives control," *IEEE-ASME Trans. Mechatron.*, vol. 27, no. 6, pp. 5560–5571, Dec. 2022.

[2] Y. Ma, D. Li, Y. Li, and L. Yang, "A novel discrete compound integral terminal sliding mode control with disturbance compensation for PMSM speed system," *IEEE-ASME Trans. Mechatron.*, vol. 27, no. 1, pp. 549–560, Feb. 2022.

[3] P. Li, L. Wang, B. Zhong, and M. Zhang, "Linear active disturbance rejection control for two-mass systems via singular perturbation approach," *IEEE Trans. Ind. Inform.*, vol. 18, no. 5, pp. 3022–3032, May 2022.

[4] Q. Zeng and J. Zhao, "Event-triggered adaptive finite-time control for active suspension systems with prescribed performance," *IEEE Trans. Ind. Inform.*, vol. 18, no. 11, pp. 7761–7769, Nov. 2022.

[5] P. Li and G. Duan, "High-order fully actuated control approaches of flexible servo systems based on singular perturbation theory," *IEEE-ASME Trans. Mechatron.*, vol. 26, no. 8, pp. 3386–3397, Dec. 2023.

[6] S. Li, Y. Xu, W. Zhang, and J. Zou, "A novel two-phase mode switching control strategy for PMSM position servo systems with fast-response and high-precision," *IEEE Trans. Power Electron.*, vol. 38, no. 1, pp. 803–815, Jan. 2023.

[7] K. J. Astrom and T. Hagglund, "Revisiting the Ziegler-Nichols step response method for PID control," *J. Process Control*, vol. 14, no. 6, pp. 635–650, Aug. 2004.

[8] H. Ozbay and A. N. Gundes, "PID and low-order controller design for guaranteed delay margin and pole placement," *Int. J. Robust Nonlinear Control*, vol. 32, no. 18, pp. 9438–9451, Dec. 2022.

[9] B. Verma and P. K. Padhy, "Indirect IMC-PID controller design," *IET Contr. Theory Appl.*, vol. 13, no. 2, pp. 297–305, Jan. 2019.

[10] M. Khamies, G. Magdy, M. Ebeed, and S. Kamel, "A robust PID controller based on linear quadratic Gaussian approach for improving frequency stability of power systems considering renewables," *ISA Trans.*, vol. 117, pp. 118–138, Nov. 2021.

[11] V. I. Utkin, *Sliding Modes in Control and Optimization.* Berlin, Germany: Springer-Verlag, 1992.

[12] T. Zeng, X. Ren, and Y. Zhang, "Fixed-time sliding mode control and high-gain nonlinearity compensation for dual-motor driving system," *IEEE Trans. Ind. Inform.*, vol. 16, no. 6, pp. 4090–4098, Jun. 2020.

[13] S. You and W. Kim, "Adaptive learning gain-based control for nonlinear systems with external disturbances: Application to PMSM," *IEEE Trans. Control Syst. Technol.*, vol. 31, no. 3, pp. 1427–1434, May 2023.

[14] Y. Zheng, H. Zhao, S. C. Zhen, and H. Sun, "Fuzzy-set theory based optimal robust constraint-following control for permanent magnet synchronous motor with uncertainties," *Control Eng. Pract.*, vol. 115, p. 104911, Oct. 2021.

[15] L. Tan, T. Cong, and D. Cong, "Neural network observers and sensorless robust optimal control for partially unknown PMSM with disturbances and saturating voltages," *IEEE Trans. Power Electron.*, vol. 36, no. 10, pp. 12045–12056, Oct. 2021.

[16] X. Zhao, S. Zhang, Z. Liu, and Q. Li, "Vibration control for flexible manipulators with event-triggering mechanism and actuator failures," *IEEE Trans. Cybern.*, vol. 52, no. 8, pp. 7591–7601, Aug. 2022.

[17] Y. Jiang, D. Shi, J. Fan, T. Chai, and T. Chen, "Event-triggered model reference adaptive control for linear partially time-variant continuous-time systems with nonlinear parametric uncertainty," *IEEE Trans. Autom. Control*, vol. 68, no. 3, pp. 1878–1885, Mar. 2023.

[18] D. Shi, J. Xue, L. Zhao, J. Wang, and Y. Huang, "Event-triggered active disturbance rejection control of DC torque motors," *IEEE-ASME Trans. Mechatron.*, vol. 22, no. 5, pp. 2277–2287, Oct. 2017.

[19] D. Shi, J. Xue, J. Wang, and Y. Huang, "A high-gain approach to event-triggered control with applications to motor systems," *IEEE Trans. Ind. Electron.*, vol. 66, no. 8, pp. 6281–6291, Aug. 2019.

[20] J. Song, D. Shi, Y. Shi, and J. Wang, "Proportional-integral event-triggered control of networked systems with unmatched uncertainties," *IEEE Trans. Ind. Electron.*, vol. 69, no. 9, pp. 9320–9330, Sep. 2022.

[21] T. Yang, X. Zhang, Y. Fang, N. Sun, and M. Iwasaki, "Observer-based adaptive fuzzy event-triggered control for mechatronic systems with inaccurate signal transmission and motion constraints," *IEEE-ASME Trans. Mechatron.*, vol. 27, no. 6, pp. 5208–5221, Dec. 2022.

[22] G. Duan, "High-order fully actuated system approaches: Part I. Models and basic procedure," *Int. J. Syst. Sci.*, vol. 52, no. 2, pp. 422–435, Jan. 2021.

[23] G. Duan, "High-order fully-actuated system approaches: Part II. Generalized strict-feedback systems," *Int. J. Syst. Sci.*, vol. 52, no. 3, pp. 437–454, Feb. 2021.
[24] G. Duan, "High-order fully actuated system approaches: Part III. Robust control and high-order backstepping," *Int. J. Syst. Sci.*, vol. 52, no. 5, pp. 952–971, Apr. 2021.
[25] D. Zhang and G. Liu, "Predictive sliding-mode control for networked high-order fully actuated multiagents under random deception attacks," *IEEE Trans. Syst. Man Cybern. Syst.*, vol. 54, no. 1, pp. 484–496, Jan. 2024.
[26] D. Zhang and G. Liu, "Robust cooperative control for heterogeneous uncertain nonlinear high-order fully actuated multiagent systems," *IEEE Trans. Cybern.*, vol. 54, no. 10, Oct. 2024.
[27] G. Tian and G. Duan, "Robust model reference tracking for uncertain second-order nonlinear systems with application to robot manipulator," *Int. J. Robust Nonlinear Control*, vol. 33, no. 3, pp. 1750–1771, Feb. 2023.
[28] G. Duan, "Fully actuated system approach for control: An overview," *IEEE Trans. Cybern.*, vol. 54, no. 12, pp. 7285–7306, Dec. 2024.
[29] P. Li and G. Duan, "High-order fully actuated control approach for servo systems based on dynamical compensator and extended state observer," *IEEE-ASME Trans. Mechatron.*, vol. 29, no. 5, pp. 3717–3726, Oct. 2024.
[30] P. Li and G. Duan, "High-order fully actuated control approaches of flexible servo systems based on singular perturbation theory," *IEEE-ASME Trans. Mechatron.*, vol. 28, no. 6, pp. 3386–3397, Dec. 2023.
[31] M. Polycarpou, "Stable adaptive neural control scheme for nonlinear systems," *IEEE Trans. Autom. Control*, vol. 41, no. 3, pp. 447–451, Mar. 1996.
[32] P. Li, K. Guo, and M. Zhang, "Linear active disturbance rejection control of servo systems via IMC principle with active damping and sliding mode techniques," *ISA Trans.*, vol. 129, pp. 663–672, Oct. 2022.
[33] J. Wang, H. Pan, and W. Sun, "Event-triggered adaptive fault-tolerant control for unknown nonlinear systems with applications to linear motor," *IEEE-ASME Trans. Mechatron.*, vol. 27, no. 2, pp. 940–949, Apr. 2022.

Ping Li (Member, IEEE) was born in Hunan Province, China, in 1989. He received the B.S. degree in mechanical engineering and automation from the South China University of Technology, Guangzhou, P.R. China, in 2011, and the Ph.D. degree in mechanical and electronic engineering from Huazhong University of Science and Technology, Wuhan, P.R. China, in 2019.

Currently, he is a Research Assistant Professor with the Southern University of Science and Technology, Shenzhen, China. His research interests include CNC system, mechatronics, system modeling and identification, servo driving control, robot motion control, and fully actuated system approach.

Guangren Duan (Fellow, IEEE) received the Ph.D. degree in control systems sciences from the Harbin Institute of Technology, Harbin, China, in 1989.

He is the Founder and the Honorary Director of the Center for Control Theory and Guidance Technology, Harbin Institute of Technology, and recently he is also In Charge of the Center for Control Science and Technology, Southern University of Science and Technology, Shenzhen, China. He visited the University of Hull, Hull, the University of Sheffield, Sheffield, and also the Queen's University of Belfast, Belfast, U.K., from 1996 to 2002. His research interests include parametric control systems design, nonlinear systems, descriptor systems, spacecraft control, and magnetic bearing control.

Dr. Duan has served as a member of the Science and Technology Committee of the Chinese Ministry of Education, Vice President of the Control Theory and Applications Committee, Chinese Association of Automation (CAA), and Associate Editor of a few international journals. Currently, he is an Academician of the Chinese Academy of Sciences, and fellow of CAA and IET.

Bi Zhang received the Ph.D. degree in mechanical engineering from Tokyo Institute of Technology, Shenyang, Japan, in 1988.

His research interests include ultra-high speed precision machining technology and equipment.

Dr. Zhang is a Russian Academy of Engineering Foreign Full Member (Academician); fellow of International Academy for Production Engineering (CIRP), American Society of Mechanical Engineers; Chair Professor of Mechanical and Energy Engineering, Associate Dean of College of Engineering, Southern University of Science and Technology, China. He is a fellow of ASME.

Yuzhong Wang (Member, IEEE) received the M.S. degree in operational research and cybernetics and the Ph.D. degree in computer software and theory from the Northeastern University, Shenyang, China, in 2018 and 2022, respectively.

From 2021 to 2022, he was a Visiting Scholar with the Nanyang Technological University, Singapore. Currently, he is a Postdoctoral Researcher with the University of Hong Kong, Hong Kong, China. His research interests include switched systems, fully actuated systems, event-triggered control, adaptive control, and sliding mode control.